

Electrochemical Model of CO₂ Corrosion in the Presence of Quaternary Ammonium Corrosion Inhibitor Model Compounds

J.M. Domínguez Olivo, B. Brown, D. Young, S. Nesic
Institute for Corrosion and Multiphase Technology
Department of Chemical & Biomolecular Engineering
Ohio University
Athens, OH 45701

ABSTRACT

The oil and gas industry utilizes surfactant-type organic corrosion inhibitors to mitigate internal pipeline corrosion. Changes in corrosion rates due to inhibitor addition have been related to adsorption isotherms as a function of the inhibitor concentration. However, the question as to how a corrosion inhibitor affects the electrochemical reactions governing CO₂ corrosion remains unclear. This research proposed to investigate the issue by using a systematic approach: four different corrosion inhibitor model compounds, synthesized in-house, were utilized to determine the effect of the tail length on the kinetics of the electrochemical process underlying the corrosion of a UNS K03014 steel in CO₂ corrosion at pH 4. The corrosion inhibitors all contained the same head group (dimethyl-benzyl-ammonium) with four different alkyl tail lengths (C4, C8, C12, and C16). A theoretical model of the increase in the activation energy of the electrochemical process underlying CO₂ corrosion due to the presence of the corrosion inhibitors led to the development of a modified Butler-Volmer equation. Such an equation describes the retardation in charge transfer rates of the electrochemical reactions associated with the corrosion of mild steel. The model was compared with experimental potentiodynamic sweeps for each system containing the corrosion inhibitor model compounds. As a result, the corrosion model predicts the corrosion rate and the open circuit potential in the presence of a corrosion inhibitor with a high degree of accuracy.

Keywords: corrosion inhibitors, alkyl tail length, mitigation, activation energy, CO₂ corrosion, mechanistic model.

INTRODUCTION

Internal corrosion of mild steel transportation pipelines is a major issue in the upstream oil and gas industry, due to the presence of produced water¹. Corrosion engineers have developed strategies to mitigate corrosion through the use of biocides, scavengers and corrosion inhibitors^{1,2}. Among those strategies, the use of organic corrosion inhibitors is one of the most widely used solutions. A corrosion inhibitor is a chemical substance that can significantly reduce corrosion of metals in particular environments when added in small concentrations¹⁻³. The oil and gas industry uses a variety of organic corrosion inhibitors to mitigate internal corrosion of pipelines. Most corrosion inhibitors are surfactant-type, such as amines, amides, and imidazolines, which primarily function by adsorbing on the metal surface and forming a barrier against corrosion^{2,4}. It is believed that those surfactant molecules primarily attach to the metal surface *via* their polar (hydrophilic) head group, while the non-polar, hydrophobic tail is assumed to be oriented perpendicular to the surface^{3,5}. Knowledge related to the efficiency and mechanism of corrosion inhibitors is usually developed by performing experiments under conditions that simulate the environment/field conditions². Generally, corrosion mitigation efficiency is measured to optimize the dosage of inhibitor added². Mathematical models are used to fit the measured efficiency to adsorption isotherms under the assumption that the coverage of the inhibitor on the metal surface is proportional to the corrosion mitigation efficiency^{2,3}. However, the key link between inhibitor alkyl tail length, surface coverage, and retardation in electrochemical kinetics has not been properly established. Questions as to how a corrosion inhibitor retards corrosion, including establishing the mechanistic role the alkyl tail plays on the processes underlying corrosion, are not fully answered.

The most commonly accepted model to describe the retardation of corrosion by a surfactant-type inhibitor in the open literature is the surface blockage effect⁶⁻⁸. This model states that corrosion inhibitors prevent electrochemical reactions by covering the metal surface⁶⁻⁸. In other words, the model implies that the area covered by the inhibitor remains uncorroded while the exposed area corrodes as if the inhibitor was not present. Although simple and widely used, the surface blockage model has numerous shortcomings. Dominguez *et al.*⁹ discussed such shortcomings and proposed a new model of inhibition from studies with corrosion inhibitor model compounds using the same head group (quaternary ammonium) and different alkyl tail lengths (butyl, octyl, dodecyl, and hexadecyl). The new model specifies that instead of blocking the surface reactions, the adsorbed corrosion inhibitor molecules only retard the charge transfer rates as the inhibitor alkyl tail displaces and replaces water molecules at the metal surface⁹. Since water facilitates the anodic dissolution of metal and hydrogen evolution in the corrosion process, water displacement induces the retardation in those charge transfer processes; this hindrance effect increases the activation energy in a measurable way⁹. The authors also concluded that a key governing factor in the inhibition process is the alkyl tail length⁹: the longer the tail length, the more effective the water displacement away from the metal surface was, and the higher the increase in the activation energy, leading to lower corrosion rates. Nevertheless, the link between the activation energy and electrochemical kinetics was not addressed in that publication. Therefore, the present paper proposes a modified Butler-Volmer equation to describe the relationship between the activation energy and kinetics in the presence of quaternary ammonium corrosion inhibitors with different alkyl tail lengths.

EXPERIMENTAL PROCEDURE

A three-electrode glass cell set up was used to conduct corrosion and corrosion mitigation experiments at 1 bar, pH 4 and 30°C. The working electrolyte was a 1 wt.% NaCl solution. A UNS K03014 API 5L X65 steel rotating cylinder electrode (RCE) at 1000 rpm was the working electrode, as shown in Figure 1. The composition of the steel is shown in Table 1. A platinum covered titanium mesh was used as a counter electrode and a KCl saturated Ag/AgCl electrode connected *via* a Luggin capillary was used as the reference. CO₂ was used to purge the system. The solution pH was adjusted and maintained at pH 4.0±0.1 during each experiment. Four different model compounds were synthesized in-house using a methodology described elsewhere⁹. The model compounds consisted of a dimethyl-benzyl-ammonium structural unit, as the head group, with four different alkyl tail lengths: 4, 8, 12 and 16 carbons (butyl, octyl, dodecyl, and hexadecyl). The working concentration for each model compound was obtained by following a previously described methodology⁹. Their respective working concentrations were the minimum concentration that yielded the maximum efficiency (also known as surface saturation concentration^{9,10}) as described in other research^{9,10}. Table 2 shows the molecular structure of the model compounds. Linear polarization resistance (LPR) was applied to obtain the charge transfer resistance by polarizing the working electrode from -5 mV to +5 mV with respect to the corrosion potential; corrosion rates were then calculated by using a *B* value of 26 mV/decade. Electrochemical impedance spectroscopy (EIS) was used for measuring solution resistance by using an oscillating potential of 10 mV rms with respect to the corrosion potential, with a frequency from 0.01 to 10,000 Hz. Cathodic potentiodynamic polarization sweeps were taken starting from the open circuit potential (OCP) to -900 mV with respect to the OCP at a scan rate of 0.1 mV/s. When the OCP was stable again (30 minutes after the end of the cathodic sweep), the anodic potentiodynamic sweep was taken from the OCP to +400 mV with respect to the OCP at a scan rate of 0.1 mV/s. The ohmic drop was accounted for in both the anodic and cathodic curves. A summary of tested conditions is given in Table 3.

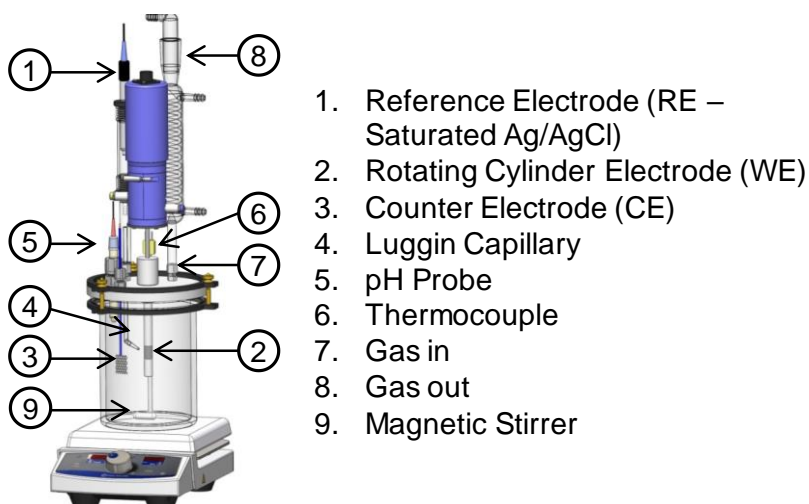


Figure 1: Three-electrode setup used to perform experiments.[†]

[†] Image courtesy of Cody Shafer, ICMT, Ohio University.

Table 1 Chemical Composition of the X65 Steel Used as the Working Electrode

| Composition | Elements | | | | | | | | | |
|-------------|----------|------|-------|-------|------|------|------|------|-------|---------|
| | Cr | Mo | S | V | Si | C | Ni | Mn | P | Fe |
| Weight % | 0.14 | 0.16 | 0.009 | 0.047 | 0.26 | 0.13 | 0.36 | 1.16 | 0.009 | Balance |

Table 2 Chemical Structure of Model Compounds

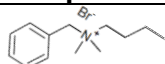
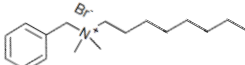
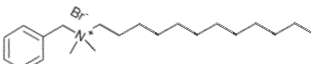
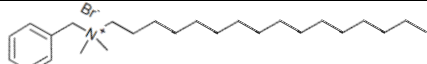
| Compound | Name |
|---|-------|
|  | Q-C4 |
|  | Q-C8 |
|  | Q-C12 |
|  | Q-C16 |

Table 3 Summary of Experimental Conditions

| Description | Parameters |
|--|---|
| Working solution | 1 wt.% NaCl |
| Sparge gas | CO ₂ |
| Temperature / °C | 30 |
| pH | 4.0 ± 0.1 |
| Corrosion inhibitors model compound concentrations | Q-C4 (200 ppm V/V) Q-C8 (150 ppm V/V) Q-C12 (100 ppm V/V) Q-C16 (50 ppm V/V) |
| Electrochemical techniques | LPR, EIS, potentiodynamic polarization |

RESULTS AND DISCUSSION

The results and discussion are comprised of three main parts. Part one discusses the development of a general electrochemical model that accounts for the changes in activation energy due to the presence of a corrosion inhibitor. The second part discusses the application of the model to the derivation of the anodic and cathodic kinetic model equations for the corrosion of mild steel. Lastly, the third part shows the validation of the electrochemical model by comparing the prediction model with experimental potentiodynamic sweeps and corrosion rates obtained with LPR.

Development of the Electrochemical Model

In a previous research article⁹ it was concluded that, given the same conditions of flow, pH, and temperature, the addition of a corrosion inhibitor increased the activation energy of the electrochemical process underlying CO₂ corrosion. A schematic representation of such an increase is depicted in Figure 2. From the idea of the increase in activation energy, a relationship that accounts for such a change in the activation energy was sought.

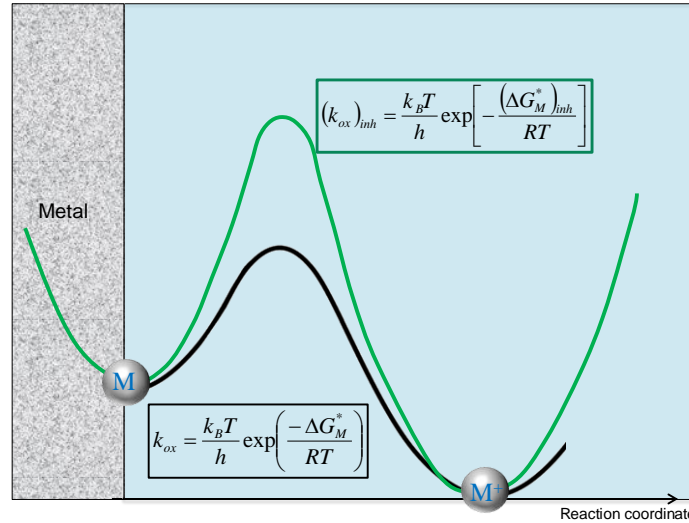


Figure 2: Increase of the activation energy for a hypothetical metal oxidation reaction. Processes at different rate constants. Green box: reaction rate in the presence of a corrosion inhibitor. Black box: reaction rate in the absence of a corrosion inhibitor. ΔG_M^* is the activation energy without inhibitor and $(\Delta G_M^*)_{inh}$ is the activation energy in the presence of a corrosion inhibitor. k_B is the Boltzmann constant, h is the Planck constant, R is the ideal gas constant and T is the absolute temperature.

Starting with the process with no corrosion inhibitor present, and according to Bockris, *et al.*¹¹, the total activation energy of multistep processes is given by Equation (1):

$$\Delta \tilde{G}_M = \Delta G_M^* + \alpha F \Delta \phi \quad (1)$$

Where:

$\Delta \tilde{G}_M$ is the total activation energy,

ΔG_M^* is the chemical component of the activation energy,

α is a charge transfer coefficient¹²,
 $\Delta\phi$ is the potential across the double layer,
 F is Faraday's constant.

In the presence of a corrosion inhibitor, the total activation energy as a function of the chemical component and the electrical component can be written as:

$$(\Delta\tilde{G}_M)_{inh} = (\Delta G_M^*)_{inh} + \alpha F \Delta\phi \quad (2)$$

where:

$(\Delta\tilde{G}_M)_{inh}$ is the total activation energy in the presence of a corrosion inhibitor,
 $(\Delta G_M^*)_{inh}$ is the chemical component of the activation energy in the presence of a corrosion inhibitor.

With Equation (1) and Equation (2), it is possible to determine a current-voltage relationship for the electrochemical processes underlying corrosion. Starting from the scenario of an electrochemical process without a corrosion inhibitor, by using an Arrhenius-type of equation¹¹ on Equation (1), the following equation is achieved:

$$i = \frac{k_B T}{h} \exp\left(-\frac{\Delta G_M^*}{RT}\right) \exp\left(-\frac{\alpha F \eta}{RT}\right) \quad (3)$$

Where:

i is the current density as a function of the overpotential,
 k_B is Boltzmann's constant,
 h is Planck's constant, and
 η is the overpotential.

Defining the exchange current density as a function of the chemical component of the activation energy yields:

$$i_0 = \frac{k_B T}{h} \exp\left(-\frac{\Delta G_M^*}{RT}\right) \quad (4)$$

Equation (3) and Equation (4) combined, can be rewritten as:

$$i = i_0 \exp\left(-\frac{\alpha F \eta}{RT}\right) \quad (5)$$

Similarly, the current-voltage relationship for the electrochemical process in the presence of a corrosion inhibitor can be obtained from Equation (2):

$$(i)_{inh} = (i_0)_{inh} \exp\left(-\frac{\alpha F \eta}{RT}\right) \quad (6)$$

where:

$(i_0)_{inh}$ is the reference exchange current density in the presence of a corrosion inhibitor defined as:

$$(i_0)_{inh} = \frac{k_B T}{h} \exp\left(-\frac{(\Delta G_M^*)_{inh}}{RT}\right) \quad (7)$$

The next step in the development of the electrochemical model is to determine the relationship between change in the reference exchange current density and the addition of a corrosion inhibitor. The change can be obtained by taking the ratio of the reference current density with and without inhibitor from Equation (4) and Equation (7). Finally, solving for the reference exchange current density for the inhibited process:

$$(i_0)_{inh} = i_0 \exp\left(-\frac{(\Delta G_M^*)_{inh} - \Delta G_M^*}{RT}\right) \quad (8)$$

Equation (8) implies that a change in exchange current density of an electrochemical process will be dependent on the difference between the activation energies of the processes (with and without inhibitor). Finally, by substituting Equation (8) into Equation (6), a model equation for charge transfer processes in the presence of corrosion inhibitors is obtained. Such an equation is a function of the change in activation energies:

$$(i)_{inh} = i_0 \exp\left(-\frac{(\Delta G_M^*)_{inh} - \Delta G_M^*}{RT}\right) \exp\left(-\frac{\alpha F \eta}{RT}\right) \quad (9)$$

Equation (9) was used to develop the charge transfer model equations for both anodic and cathodic processes of the acidic corrosion of mild steel. The process is described in the following section.

Development of the Model Equations

It must be noted that the model equations are subjected to the following assumptions:

- The metal surface is uniformly corroding with no corrosion products formed (no iron carbide or iron carbonate formed).
- The inhibitor adsorbs uniformly on the metal surface: both anodic and cathodic kinetics are equally affected by the corrosion inhibitor (no preferential adsorption).

As proven in previous research¹³:

- The inhibitor affects only charge transfer kinetics.
- Diffusion and chemical reaction processes are unaffected by the presence of the corrosion inhibitor (*i.e.*, diffusion-controlled and chemically-controlled limiting currents do not change).

Anodic Reaction

The dissolution of iron is the dominant anodic reaction in corrosion¹⁴. Since the reaction is under charge transfer control¹⁵, the model equation for this reaction was obtained as:

$$(i_{ct}^a)_{inh} = (i_0^a) \exp\left(-\frac{(\Delta G_M^*)_{inh} - \Delta G_M^*}{RT}\right) \exp\left(-\frac{1.5F\eta_a}{RT}\right) \quad (10)$$

where:

η_a is the anodic overpotential ($\eta_a > 0$),

1.5 is the charge transfer coefficient for this multistep reaction previously defined by Bockris, *et al.*¹⁴

Cathodic Reactions

For the corrosion process of steel in acidic conditions, the dominant cathodic reaction is hydrogen evolution¹⁵. For the charge transfer process resulting in hydrogen evolution, the charge transfer coefficient is 0.5¹⁴. The model equation was obtained as:

$$(i_{ct}^c)_{inh} = (i_0^c) \exp\left(-\frac{(\Delta G_M^*)_{inh} - \Delta G_M^*}{RT}\right) \exp\left(-\frac{0.5F\eta_c}{RT}\right) \quad (11)$$

The following equation can be used¹⁵ to include limiting currents (unaffected by the presence of organic corrosion inhibitors) into the overall current density calculation:

$$\frac{1}{(i^c)_{inh}} = \frac{1}{(i_{ct}^c)_{inh}} + \frac{1}{i_{lim}} \quad (12)$$

The water reduction line was included as part of the kinetic model with a model equation similar to Equation (11) since the addition of inhibitor also retards this reaction.

Validation of the Model Equations

Equation (10), Equation (11) and Equation (12) were validated by comparing experimental potentiodynamic sweeps with the model equations. The activation energies used for the model were previously reported⁹ and are summarized in Table 4.

Table 4 Activation Energy for Systems Containing Corrosion Inhibitor Model Compounds

| System | Activation Energy kJ mol ⁻¹ |
|--------------|---|
| no inhibitor | 48 |
| Q-C4 | 50.5 |
| Q-C8 | 52.3 |
| Q-C12 | 53.4 |
| Q-C16 | 55.9 |

The first model compound to be compared was Q-C4. As seen in Figure 3, the model equations predicted with reasonable accuracy the rates of the charge transfer electrochemical reactions (anodic and cathodic). The “H⁺ Reduction”, “Fe Dissolution,” and “H₂O Reduction” lines in the figures are shown as calculated by the model in the presence of the corrosion inhibitor. It must be noted that not only is the electrochemical

reaction predicting the corrosion rate, the corrosion potential is also well predicted by the electrochemical model.

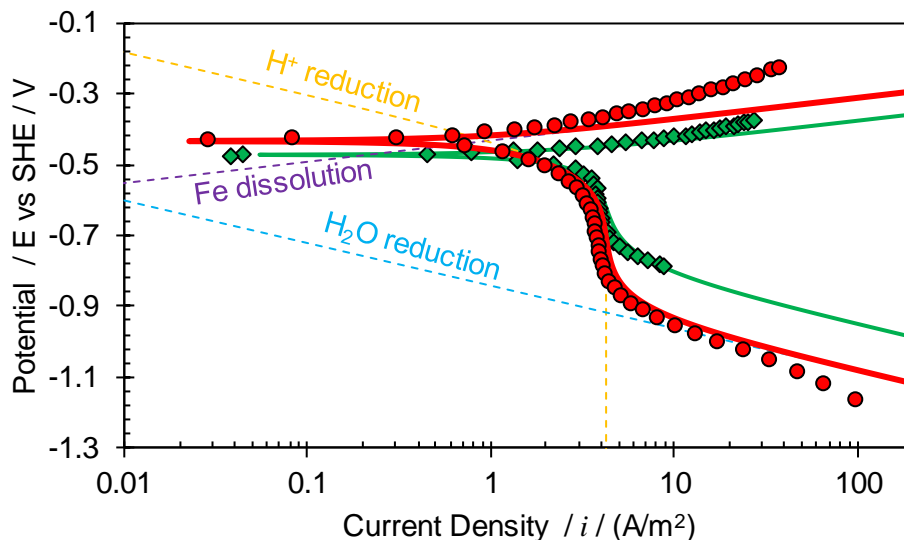


Figure 3: Comparison of experimental potentiodynamic sweeps (markers) with the developed model (solid lines). Square green marker and green line: CO₂ with no corrosion inhibitor. Red rounded markers and red line: CO₂ in the presence of corrosion inhibitor model compound Q-C4. Experimental conditions: 30°C, pH 4, 1000 rpm RCE.

In the same way, the electrochemical model was compared to the potentiodynamic polarization curves with the corrosion inhibitor model compound Q-C8.

Figure 4 shows a good agreement between the experimental and the predicted electrochemical kinetics.

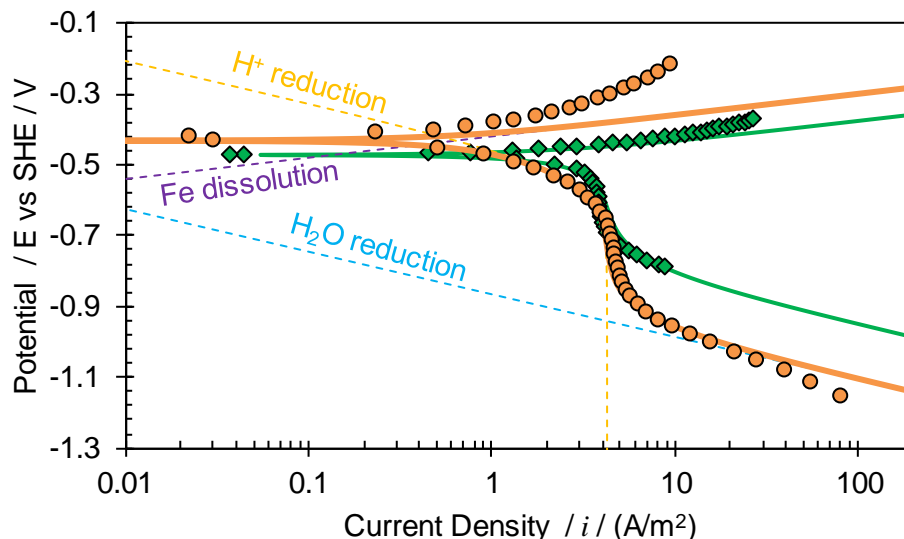


Figure 4: Comparison of experimental potentiodynamic sweeps (markers) with the developed model (solid lines). Square green marker and green line: CO₂ with no corrosion inhibitor. Orange rounded markers and the orange line: CO₂ in the presence of corrosion inhibitor model compound Q-C8. Experimental conditions: 30°C, pH 4, 1000 rpm RCE.

The same comparison was done for the corrosion inhibitor model compound Q-C12, with good results in the prediction of the electrochemical kinetics. The comparison can be seen in Figure 5.

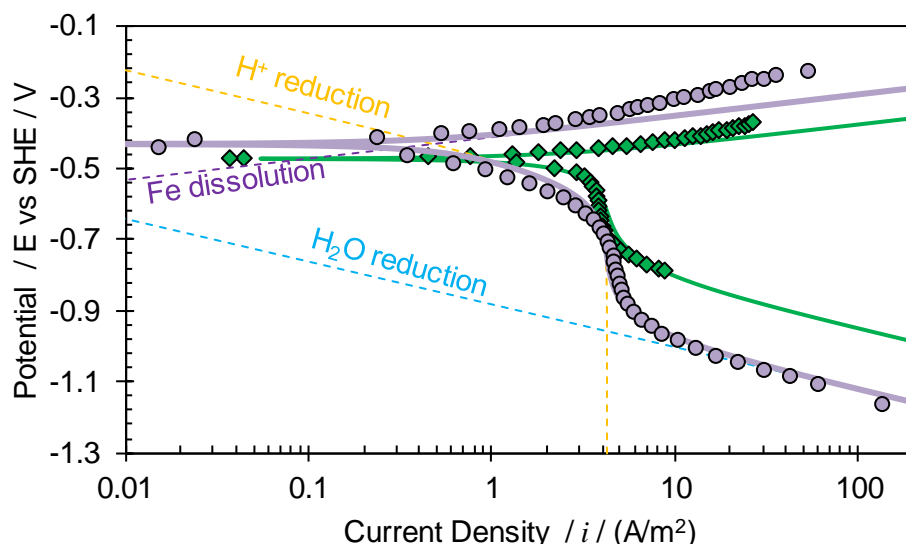


Figure 5: Comparison of experimental potentiodynamic sweeps (markers) with the developed model (solid lines). Square green marker and green line: CO_2 with no corrosion inhibitor. Purple rounded markers and the purple line: CO_2 in the presence of corrosion inhibitor model compound Q-C12. Experimental conditions: 30°C , pH 4, 1000 rpm RCE.

Finally, the experimental potentiodynamic curves for the inhibitor model compound Q-C16 were compared to the developed electrochemical model (Figure 6).

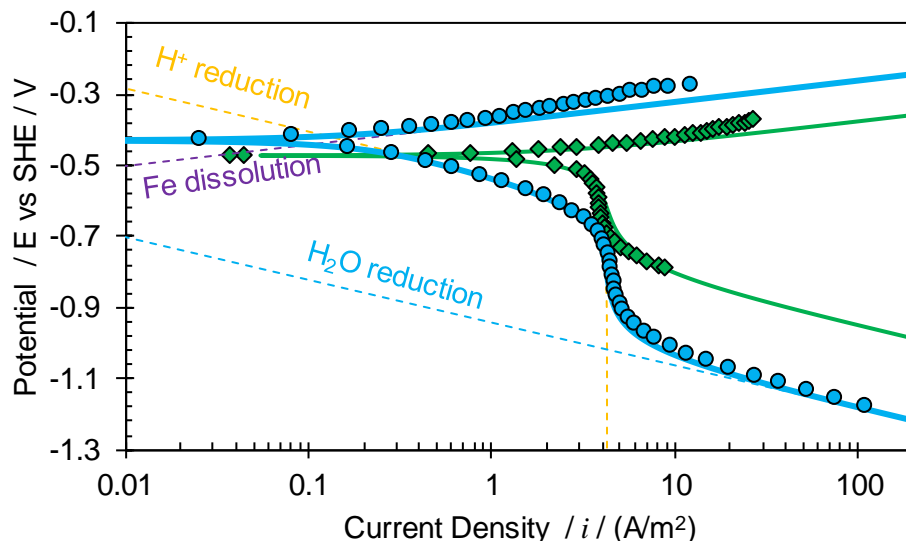


Figure 6: Comparison of experimental potentiodynamic sweeps (markers) with the developed model (solid lines). Square green marker and green line: CO_2 with no corrosion inhibitor. Blue rounded markers and the blue line: CO_2 in the presence of corrosion inhibitor model compound Q-C16. Experimental conditions: 30°C , pH 4, 1000 rpm RCE.

A comparison between experimental and predicted corrosion rates, as well as the changes in corrosion potential, are shown in Figure 7 and Figure 8. A good agreement between the model and the LPR experimental data was found.

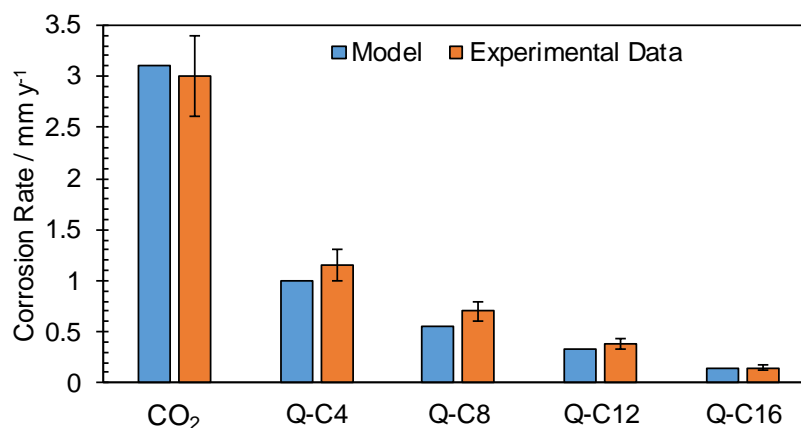


Figure 7: Comparison of LPR corrosion rates with those predicted with the proposed electrochemical model. Error bars: Maximum and minimum values obtained. Experimental conditions: 1 bar pCO₂, 30°C, pH 4, 1000 rpm RCE.

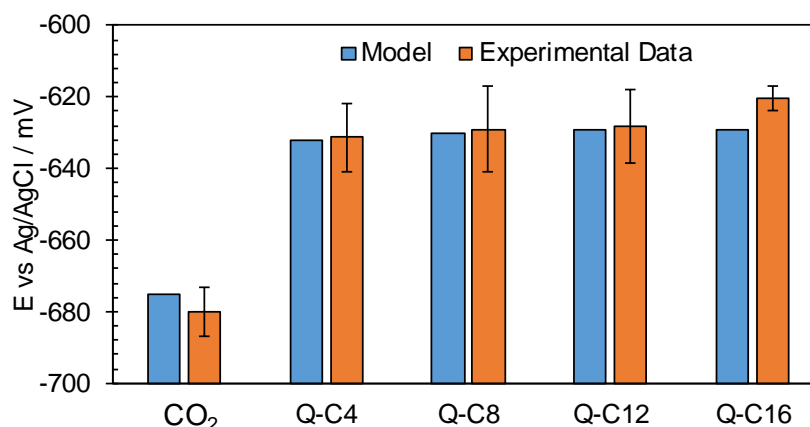


Figure 8: Comparison of experimental corrosion potential with those predicted with the proposed electrochemical model. Error bars: Maximum and minimum values obtained. Experimental conditions: 1 bar pCO₂, 30°C, pH 4, 1000 rpm RCE.

CONCLUSIONS

- The corrosion model predicts the corrosion rate and the open circuit potential in the presence of a corrosion inhibitor with a high degree of accuracy.
- A modified Butler-Volmer equation for the charge transfer processes affected by the presence of a corrosion inhibitor was developed.
- The model is based on the assumption that there is a change in the activation energy of the charge transfer process due to water displacement by the adsorbed corrosion inhibitor. Higher activation energies led to slower charge transfer reaction rates and, consequently, lower corrosion rates.

ACKNOWLEDGMENTS

The authors would like to thank the following companies for their financial support: Anadarko, Baker Hughes, BP, Chevron, CNOOC, ConocoPhillips, DNV GL, ExxonMobil, M-I SWACO (Schlumberger), Multi-Chem (Halliburton), Occidental Oil Company, PTT, Saudi Aramco, SINOPEC (China Petroleum), and TOTAL.

REFERENCES

1. D. A. Jones, *Principles and prevention of corrosion*, 2nd ed. (New York, NY: MacMillan, 1996), pp. 503-570.
2. H.H. Uhlig (Editor), *Uhlig's Corrosion Handbook*, 3rd ed. (Hoboken, NJ: John Wiley & Sons, Inc.), pp. 1021-1032.
3. E. McCafferty, *Introduction to corrosion science*, (New York, NY: Springer, 2010), pp. 359-400.
4. V. S. Sastri, *Green Corrosion Inhibitors*, 2nd ed. (Hoboken, NJ: John Wiley & Sons, 2011), p. 110.
5. A. Edwards, C. Osborne, S. Webster, D. Klenerman, M. Joseph, P. Ostovar, and M. Doyle, "Mechanistic studies of the corrosion inhibitor oleic imidazoline," *Corrosion Science* 36, 2, (1994): pp. 315–325.
6. W. J. Lorenz and F. Mansfeld, "Interface and interphase corrosion inhibition," *Electrochimica Acta* 31, 4, (1985): pp. 467–476.
7. C. Cao, "On electrochemical techniques for interface inhibitor research," *Corrosion Science* 38, 12, (1996): pp. 2073–2082.
8. M. Palomar-Pardavé, M. Romero-Romo, H. Herrera-Hernández, M.A. Abreu-Quijano, N. V. Likhanova, J. Uruchurtu, and J.M. Juárez-García, "Influence of the alkyl chain length of 2 amino 5 alkyl 1,3,4 thiadiazole compounds on the corrosion inhibition of steel immersed in sulfuric acid solutions," *Corrosion Science* 54, 1, (2012): pp. 231–243.
9. J.M. Dominguez Olivo, D. Young, B. Brown, S. Nesic, "Effect of corrosion inhibitor alkyl tail length on the electrochemical process underlying CO₂ corrosion of mild steel," NACE Corrosion Conference 2018, paper 11537 (Houston, TX: NACE, 2018).
10. T. Murakawa, S. Nagaura, and N. Hackerman, "Coverage of iron surface by organic compounds and anions in acid solutions," *Corrosion Science* 7, 2, (1967): pp. 79–89.
11. J. O. Bockris, A. K. N. Reddy, and M. Gamboa-Adelco, *Modern Electrochemistry 2A, Fundamentals of Electrodics*, (New York, NY: Springer, 2001), pp. 1–817.
12. J. O. Bockris and Z. Nagy, "Symmetry factor and transfer coefficient. A source of confusion in electrode kinetics," *Journal of Chemical Education* 50, 12, (1973): pp. 839-843.
13. J. M. Dominguez Olivo, B. Brown, and S. Nesic, "Modeling of corrosion mechanisms in the presence of quaternary ammonium chloride and imidazoline corrosion inhibitors," NACE Corrosion Conference 2016, paper 7406 (Houston, TX: NACE, 2016).
14. J. O. Bockris, D. Drazic, and A. Despic, "The electrode kinetics of the deposition and dissolution of iron," *Electrochimica Acta* 4, (1961): pp. 325-361.
15. M. Nordsveen, S. Nesic, R. Nyborg and A. Stangeland "A mechanistic model for carbon dioxide corrosion of mild steel in the presence of protective iron carbonate films – part 1: theory and verification," *Corrosion* 59, 5, (2003): pp. 443-456.